Vision Research 161 (2019) 18–24

Contents lists available at ScienceDirect

Vision Research

journal homepage: www.elsevier.com/locate/visres

Stimulus information supporting bilateral symmetry perception

Ilmari Kurki

Department of Psychology and Logopedics, Faculty of Medicine, PO Box 63, University of Helsinki, Finland

ARTICLE INFO

Keywords:
Bilateral symmetry
Texture perception
Classification image
Spatial vision

ABSTRACT

A classification image (a psychophysical reverse-correlation) method was used to investigate what stimulus regions and information the visual system uses for bilateral symmetry perception. The stimuli were symmetric random-dot patterns with either low or high dot density. First, the spatial integration region supporting symmetry perception was estimated, by analyzing the trial-to-trial correlation between the spatial location of symmetric dots and the corresponding response. It was observed that the integration region was rather compact (3 deg^2 with dense stimulus), vertically elongated and located near to the axis of symmetry. The size of the area was dependent on the pattern density, being larger with low-density stimulus. Next, the resolution of the symmetry matching was probed by estimating how close to the perfect symmetry the dots in two stimulus parts must be to be perceived as symmetric (classification image for symmetry tolerance). Dot pairings up to 6 arc min off from the mirror symmetry correlated with symmetry response, suggesting that the process underlying symmetry matching has large tolerance and low resolution. Outside the integration region, the symmetry tolerance classification image weights were essentially zero, suggesting that the lack of symmetry integration there is not a byproduct of high tolerance.

1. Introduction

1.1. Bilateral symmetry perception

Analysis of bilateral (mirror) symmetry is assumed to have significant functions in human perception (for a review, see Bertamini, Silvanto, Norcia, Makin, & Wagemans, 2018; Treder, 2010; van der Helm, 2015; Wagemans, 1997). Symmetry is assumed to be an important cue in early perceptual organization and grouping. Gestalt psychologists proposed that symmetric shapes are seen more readily as figures rather than ground (Bahnsen, 1928). More recent studies have shown that symmetric contours are easier to detect among randomly oriented background elements than asymmetric contours (Machilsen, Pauwels, & Wagemans, 2009). On a more theoretical level, it is possible that as symmetry is non-accidental property of biological and artificial stimuli, the visual system uses symmetry as an indicator for these objects. Since many objects such as animals and plants have a single axis of bilateral symmetry, mirror symmetry might also be used to determine the canonical axis of an object for further recognition (van der Helm, 2015). Further symmetry is widely used in visual art and architecture. It has also been proposed that analysis of facial and body symmetry may have a significant biological function in mating (Rhodes, 2006).

It is not clear whether symmetry is processed at early or late neural processing stage. Symmetry can be perceived effortlessly even in random-dot or noise textures that do not contain any meaningful shape information. Symmetry perception is possible in presentations of under 50 ms (Julesz, 1971) and symmetry perception seems to be rather sensitive to “low-level” stimulus properties such as orientation content. Horizontal and vertical mirror symmetries are easier to perceive than “oblique” (Barlow & Reeves, 1979; Jenkins, 1985; Wenderoth, 1997), similarly to well-known low-level orientation sensitivity in early vision. Symmetry perception is sensitive to stimulus spatial frequency spectrum of symmetric image parts (Dakin & Herbert, 1998; Rainville & Kingdom, 2002). These results suggest that symmetry perception has some characteristics similar to what has been generally attributed to early visual processing stages. On the other hand, it is known that early stages of the visual system process information very locally whereas evaluation of image symmetry requires the comparison of stimulus elements over larger distances. fMRI neural imaging studies have shown symmetry-related activation in extrastriate visual areas, such as lateral occipital (LO) cortex and V4 that are associated with mid-level shape and object processing, whereas earlier visual areas show little sensitivity for symmetry (Sasaki, Vanduffel, Knutsen, Tyler, & Tootell, 2005; Tyler et al., 2005). A recent TMS study also suggests that activation in the LO is causally involved in symmetry perception (Bona, Herbert, Toneatto, Silvanto, & Cattaneo, 2014). Similar results about spatial integration processes that are specific to symmetry perception

E-mail address: ilmari.kurki@helsinki.fi.

https://doi.org/10.1016/j.visres.2019.02.017
Received 10 October 2018; Received in revised form 20 February 2019; Accepted 20 February 2019
Available online 12 June 2019

have been obtained in a recent study using frequency-tagged EEG (Alp, Kohler, Kogo, Wagemans, & Norcia, 2018).

In this study, an approach based on classification image or psychophysical reverse correlation (see e.g. Beard & Ahumada, 1998; Eckstein & Ahumada, 2002; Neri, Parker, & Blakemore, 1999; for a review, see Murray, 2011) was used to estimate what stimulus parts and features the visual system uses for symmetry perception. The stimuli in classification image experiment are stochastic (here: random dots) and the observer's task is to detect the target (symmetric random dots among random dots; 50% of the trials) among noise trials (entirely random dots). The proportion of symmetric dots is set so that the task is at detection threshold (i.e. 75% correct responses). The region of the stimulus that the visual system uses for symmetry responses is then estimated by correlating the location of symmetric dots in each trial with the corresponding symmetry responses. Intuitively, if a certain location is used for symmetry evaluation, then a positive correlation between presence of symmetric dots in that position and the response should be seen, whereas if location is not used then the correlation should be zero. The results can be visualized as a classification image, a map that shows the sensitivity across the stimulus space.

Previous studies have estimated the critical stimulus region for symmetry or "symmetry integration region" by varying the size and spatial location of the region containing the symmetric stimulus. Barlow and Reeves (1979) showed that sensitivity for bilateral symmetry in random dots was highest when the symmetry signal was near the axis of symmetry, lower when symmetric dots were placed at the edges of the display and lowest, when the symmetric dots were at the intermediate locations. Other studies have shown that this integration region might be as small as a few degrees (Jenkins, 1982). It has been proposed that the integration region has an anisotropic shape, being elongated in the direction of the axis of symmetry (Dakin & Herbert, 1998). Classification images allows a "direct" estimation of the symmetry integration region without parametrically changing the signal area parameters, as in many previous experiments. The classification image approach thus does not need assumptions about the shape of integration area (e.g. circular and centered to fovea). Moreover, the size of the signal area can be held constant, whereas it varies in the parametric approach. This could lead to an estimation bias if the subjects would change their integration region with signal area (e.g., integrating mostly on the outer stimulus border).

Previous studies have also suggested that the integration region might not be fixed, but may scale with the spatial frequency of the stimulus (Dakin & Herbert, 1998). It has been proposed that the integration region would be directly related to the number of stimulus elements: Rainville and Kingdom (2002) measured tolerance for symmetry jitter by varying the density, numerosity, and size of the stimulus. By comparing the jitter thresholds in various conditions, it was concluded that the size of the integration region scales with stimulus density, being larger for sparse stimuli. Moreover, they found that the number of stimulus elements within the integration region stays approximately constant and is estimated to be approximately 18. Using the classification image method here provides a more straightforward way to estimate the size of the integration region and to test this hypothesis.

In addition, a novel "symmetry tolerance" classification image analysis was performed to investigate the selectivity and tolerance of the symmetry matching process, or close to the perfect mirror symmetry the dots in the two stimulus parts must be to be perceived as mirror symmetric. Previous studies have shown that perception of symmetric random-dot patterns is tolerant to large spatial jitter in element positions (Barlow & Reeves, 1979). This would suggest that unlike an ideal observer that would consider only the perfectly symmetrical image parts for the symmetry estimate, the human visual system would operate at a lower spatial resolution and have larger tolerance for close-to-symmetric image parts. Large tolerance increases the versatility and tolerance for symmetry perception as many natural objects such as faces are only approximately symmetrical. On the other hand, large tolerance would decrease the specificity of mirror symmetry detection, as non-symmetric image parts would cause false symmetry matches. Larger tolerance would therefore also predict less efficient detection of symmetry. An ideal mirror-symmetry detector would match only perfectly symmetric dots.

The symmetry tolerance classification image analysis allows a more detailed view of how close-to-symmetric structures are matched in the visual system by estimating how close-to-symmetric structures contribute to symmetry responses. The number of perfectly symmetric as well as close-to-symmetric dots pairs (i.e. dots that were 1,2,… pixels offset from mirror symmetry) in each stimulus were first computed for each offset. This distribution in each trial was then correlated with the symmetry response in the corresponding trial. The correlation between the dots of different degrees of symmetry and symmetry response can be used to estimate the symmetry classification image that shows the tolerance range. An ideal observer would consider only perfectly symmetric dots, showing no correlation with close-to-symmetric dots. If the matching process would have a small tolerance, that would show up in the symmetry matching classification image as positive correlation with small offsets. On the other hand, if symmetry matching has large tolerance, symmetry tolerance classification image would show correlation even with large offsets.

A tolerance classification image was estimated separately for inside and outside the estimated integration region. The rationale here was to investigate if the tolerance is constant across the stimulus or if it varies with eccentricity. One possibility is that an integration region would be in fact just a manifestation of a progressively increasing symmetry matching tolerance (or decreasing resolution). In this scheme, the resolution for the peripheral matching would be so low, and correspondingly efficiency would be so low such that it would look like contributing nothing to symmetry responses.

2. Methods

2.1. Subjects

Seven Subjects (5 females; age range 22–39) participated in the experiments. All except one (IK) were naïve about to the purposes of the study. IK, SS and CK were experienced psychophysical observers whereas NE, ML, NS and AO were new to psychophysical experiments and were included to ensure that the results can also be achieved also without extensive practice in experiments. The number of subjects was chosen based on available volunteers and is equal to or larger than in many comparable studies that use the classification image method.

The experimental procedure was designed in accordance with the Declaration of Helsinki and was approved by the Ethics Committee of the Institute of Behavioural Sciences, University of Helsinki. All subjects were volunteers and gave their informed written consent to participate. Unexperienced subjects received small compensation for participating in study.

2.2. Apparatus and stimuli

Experiments were performed in a dimly-lit laboratory. Stimuli were created using Matlab 2013b (Mathworks Inc., Natick, MA) using custom software and PsychToolbox 3 extensions (Brainard, 1997; Kleiner, Brainard, & Pelli, 2007; Pelli, 1997). Stimuli were displayed on a Mitsubishi Diamond Pro 2070 SB monitor. The monitor had a display area of 38 × 28.5 cm, 11.2 × 8.38 deg and maximum luminance of 100 Cd/m^2. Screen resolution was 800 × 600 pixels, but each pixel was rescaled horizontally and vertically by a factor of 4, the effective resolution (and the resolution of the data) was thus 200 × 160 pixels.

A Cambridge Research Systems (Cambridge, UK) ViSaGe MK II stimulus generator with 15-bit luminance resolution was used to display the stimuli. The viewing distance was 200 cm, controlled by a chin rest.

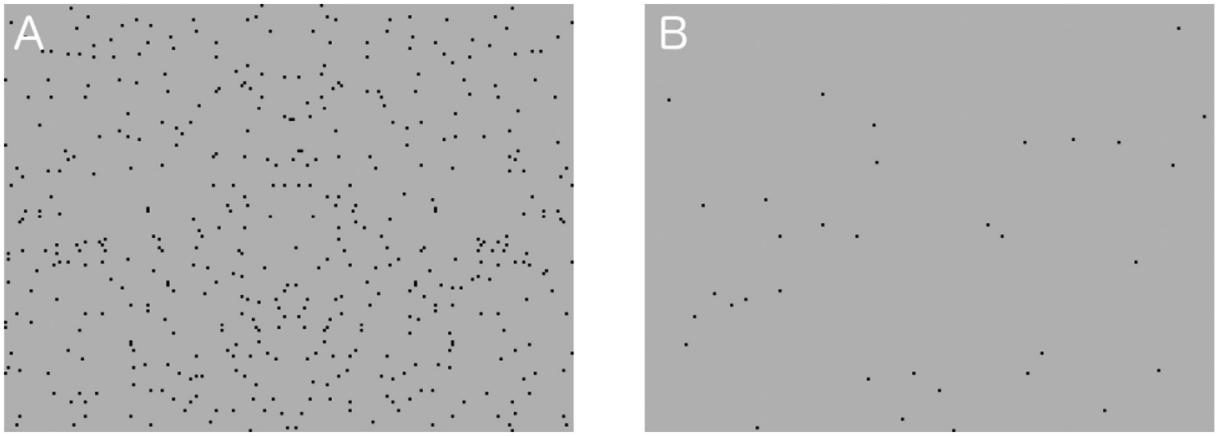

Fig. 1. Stimuli. Left: an example of dense stimulus with 50% symmetry target. Right: an example of sparse stimulus with no target (purely random dots).

Stimuli were black random-dot patterns displayed on a gray uniform background that had 75% of the maximum luminance. The size of the rectangular dots was 3.35 × 3.35 arc min (see Fig. 1). The rationale for using dots instead of spatially continuous band-pass patterns here was to maximize the contrast and visibility of the elements across the screen and maximizing the range of achievable dot densities. Another reason for using discrete dots was that they did not have potential problems in element overlap which could have covaried with density. Two texture (dot) densities were tested in separate conditions. In the dense, experiment condition dot density was 5.01 dots/deg^2; in the sparse condition, dot density was 0.391 dots/deg^2. The random-dot stimulus covered the whole (rectangular) display area. A part of the random dots in the target stimulus was mirrored with respect to the axis of the mirror symmetry, which was always at the vertical midline of the screen.

2.3. Procedure

A trial started with presentation of central fixation for 250 milliseconds (ms), followed by a blank screen for 250 ms. Stimulus was then presented for 400 ms. In 50% of the trials the stimulus was a target that contained a proportion of mirror-symmetric random dots among random dots. In the remaining trials, all dots were randomly positioned. Subjects indicated whether the stimulus was a symmetric target or not by using a keyboard. Auditory feedback was given from incorrect responses. The next trial started immediately after the response. The proportion of symmetric dots among the random dots in the target stimulus (signal-to-noise ratio) was varied using the QUEST method (Watson & Pelli, 1983) so that the subjects made on average 75% correct choices.

Sparse and dense experiments were run in a randomized order. One experiment run consisted of 120 trials of a single condition. The total number of trials per condition was 8880 (CK, IK, SS) or 2880 (subjects NE, ML, NS, AO). The total duration of the experiments was from 4 to 12 h, run over several days. Observers practiced with the task and stimuli using highly symmetrical stimuli before starting the main experiment.

2.4. Data analysis

2.4.1. Detection performance analysis

Detection performance for each condition was defined as the percentage of symmetric dots at the 75% detection threshold (signal-to-noise ratio). This was computed from the mean of the Quest threshold estimates for each run.

2.4.2. Classification image for the integration region

Classification image C was estimated using a straightforward weighted means approach (see for example: Ahumada, 2002) as symmetric dots are independently and uniformly distributed. Locations of symmetric dots were first analyzed for every stimulus (half), resulting in a Boolean matrix S that mapped the presence of symmetry in every stimulus location. The classification image was then computed by comparing the average number of symmetric dots in each location in trials where the subject reported symmetry ($r1$) to that of trials where subject reported no symmetry ($r0$):

$$C = \bar{S}_{s1r1} - \bar{S}_{s1r0} \quad (1)$$

where the line operator denotes the arithmetic average. Only the target trials ($s1$) were used in this analysis. The classification image shows the correlation between symmetry in each stimulus location and symmetry response; if it is assumed that the visual system integrates symmetry signals linearly but with varying sensitivity across the visual field, correlations in the classification image can be considered as "weights" that describe the sensitivity for the symmetry in that location (see for example: Ahumada, 2002).

This same analysis could also have been performed for the noise trials. However, the results were found to be very noisy, probably because the proportion of perfectly symmetric random dots was rather small.

The resulting classification image was spatially averaged (smoothed), to improve the signal-to-noise ratio. This was done using a [6 × 6] pixel uniform convolution kernel. Bootstrap resampling (Efron & Tibshirani, 1993) was then used to estimate the statistical significance of the convoluted classification image. 10,000 Bootstrap replicas were generated by randomly sampling (with replacement) the stimuli, keeping the total number of trials and number of responses the same as in the experiment. The classification image was computed for each replica and convoluted. One p-value for each (statistically independent) [6 × 6] block of stimulus was obtained using the distribution of Bootstrap replicas and the exact test. Finally, the p-values were corrected for multiple comparison using the false discovery rate procedure (Benjamini & Hochberg, 1995) at a family-wise error rate of 5%. For the grand average classification image, p-values were computed using a paired t-test. Other aspects of the statistical analysis were the same.

The dimensions of the integration region were quantified by fitting a two-dimensional, 4-parameter (amplitude, vertical center, width, height) Gaussian function to the classification image using the least-squares procedure. The **fminsearch** function of Matlab was used for optimization.

2.4.3. Classification image for symmetry tolerance

The first step in the tolerance analysis was to analyze the number of symmetric and close-to-symmetric dot pairs in each stimulus. This was done using two-dimensional spatial cross-correlation between all dots in one stimulus part (half) and the vertically flipped version of the matching other stimulus part. More specifically, for the stimulus (a binary-valued matrix representing the dots) in each trial k, a two-dimensional symmetry cross-correlation D_t was computed by cross-correlating the left part of the stimulus L and a horizontally flipped copy of the right part R, R^F for a range of vertical Δy and horizontal Δx pixel offsets from d_x to d_y:

$$D_k(\Delta x, \Delta y) = \sum_{x=-d_x}^{d_x} \sum_{y=-d_y}^{d_y} L_k(x, y) R_k^F(x + \Delta x, y + \Delta y) \quad (2)$$

This symmetry cross-correlation returns the number of "matching" symmetric dots for each horizontal and vertical offset (i.e. the number of dots that would be symmetric, if translated by the offset). The zero offset corresponds to the number of perfectly symmetric dots.

The classification image for symmetry tolerance were estimated separately from different parts of the stimulus, from inside and outside of the integration region.

Before calculating the cross-correlation, one of the stimulus parts (left) was windowed with a semicircular window (outer radius 3.35°) that was centered at the horizontal midline of the stimulus. For the same analysis outside of the integration region, a semiannular mask was used (inner radius 3.35°). The size of the window defining the central region was constant in all subjects, and chosen so that it was slightly larger than the largest estimated integration region.

The next step was to correlate the symmetry cross-correlation with the symmetry-responses. A generalized linear model (Knoblauch & Maloney, 2008) was used since the cross-correlation statistics is not strictly independent as each dot is a member in several cross-correlations (the correlations were however rather weak < 0.15). A simple weighted means might be sensitive for this covariance, and therefore a generalized linear model where this covariance is incorporated into the model was used. In more detail, Matlab's **mnrfit** function was used to implement a generalized linear ordinal probit model (for a review see: Knoblauch & Maloney, 2012). The analysis estimates how strongly the number of different degrees of close-to-symmetric dots (from −9 to +10 pixels offset from perfect symmetry; 40 regressors) contribute to the symmetry response (dependent variable; 4 levels). Only data from no-target trials was used. As the data were rather noisy, the data from all subjects were pooled together. To further increase the signal-to-noise ratio, a radial average (the average value as a function of distance from the origin) of the classification image for symmetry tolerance was computed. Only the trials without the target (only random dots) were used for this. This ensured that the symmetrical target signal would not bias the results. Simulations were used to ensure that this method estimates tolerance reasonably well.

3. Results

3.1. Symmetry detection performance

Dot density did not have a systematic effect on detection performance. The percentage of symmetric dots at the threshold was on average 56.9% (standard deviation [SD] across the subjects 5.7%) in the dense and 58.7% (SD 7.6%) in the sparse condition (Fig. 2). However, most subjects showed systematically better detection performance in one of the conditions, for example CK had a lower threshold in the sparse ($t(73) = 6.298$; $p < 0.001$) and NE in the dense condition ($t(23) = 6.244$; $p < 0.001$).

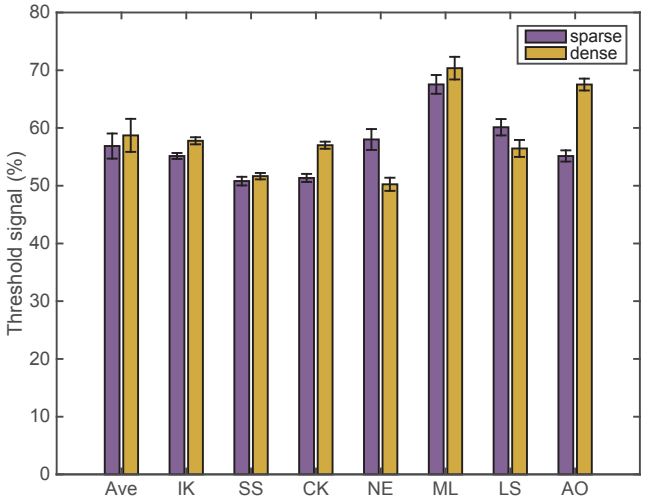

Fig. 2. Mean threshold signal (percentage of symmetric dots) in sparse and dense conditions. Ave refers to the average of subjects. Error bars represent 1 standard error of mean, obtained by Bootstrap resampling.

3.2. Integration region classification image

Symmetry integration classification image shows that sensitivity for symmetry is high in limited region located at the center of the stimulus (Fig. 3) and generally low at more peripheral locations. With one exception (AO, sparse condition) this integration region is well fitted by an oval, Gaussian function that peaks at the location of the symmetry axis. AO's sparse condition showed an atypical strategy that does not result in a clear integration region. This subject seems to integrate from wide regions located to the top edge of the stimulus. Since this strategy was not well captured by a Gaussian function, subject's data was excluded from further analyses.

The integration region is elongated along the vertical axis (axis of symmetry). The average aspect ratio was 2.57 in the dense condition and 1.27 in the sparse condition (t-test for the unity of aspect ratio, using pooled data from both conditions: $t(11) = 2.49$; $p = 0.03$; Cohen's $d_z = 0.717$). Interestingly, the integration region is on average more circular in the sparse condition. However there is considerable variation in the aspect ratio, and the difference was not statistically significant ($t(5) = 2.07$, $p > 0.05$, $d_z = 0.797$; for the individual data, see Table 1).

The integration region was clearly larger in the sparse condition, on average about 3.5 times the area of the dense condition (9.33 versus 2.64 deg^2; $t(5) = 5.24$; $p = 0.003$; $d_z = 1.95$). The average width of the integration region was larger, 0.60 deg in the dense condition and 1.52 deg in the sparse condition ($t(5) = 7.81$; $p < 0.001$; $d_z = 2.86$). The difference in height was not statistically significant ($t(5) = 1.56$; $p > 0.05$; $d_z = 0.612$).

3.3. Symmetry tolerance classification image

The symmetry tolerance classification images (Fig. 4) probes the resolution of the matching process, by showing how close-to-symmetric dots correlate with symmetry responses. Insets show the tolerance classification images estimated from the stimulus inside and outside the estimated integration region. Plots show the radial average. The results in both dense and sparse conditions show that tolerance for symmetry is rather large: a range of close-to-symmetric dot pairings up to 4 arc min in the dense condition and up to 6 arc min in the sparse condition correlated with symmetry responses. Tolerance area outside the integration region in the dense condition indicates that perfectly symmetric dots may have some contribution, but otherwise the results show no evidence of using symmetric or close-to-symmetric structures.

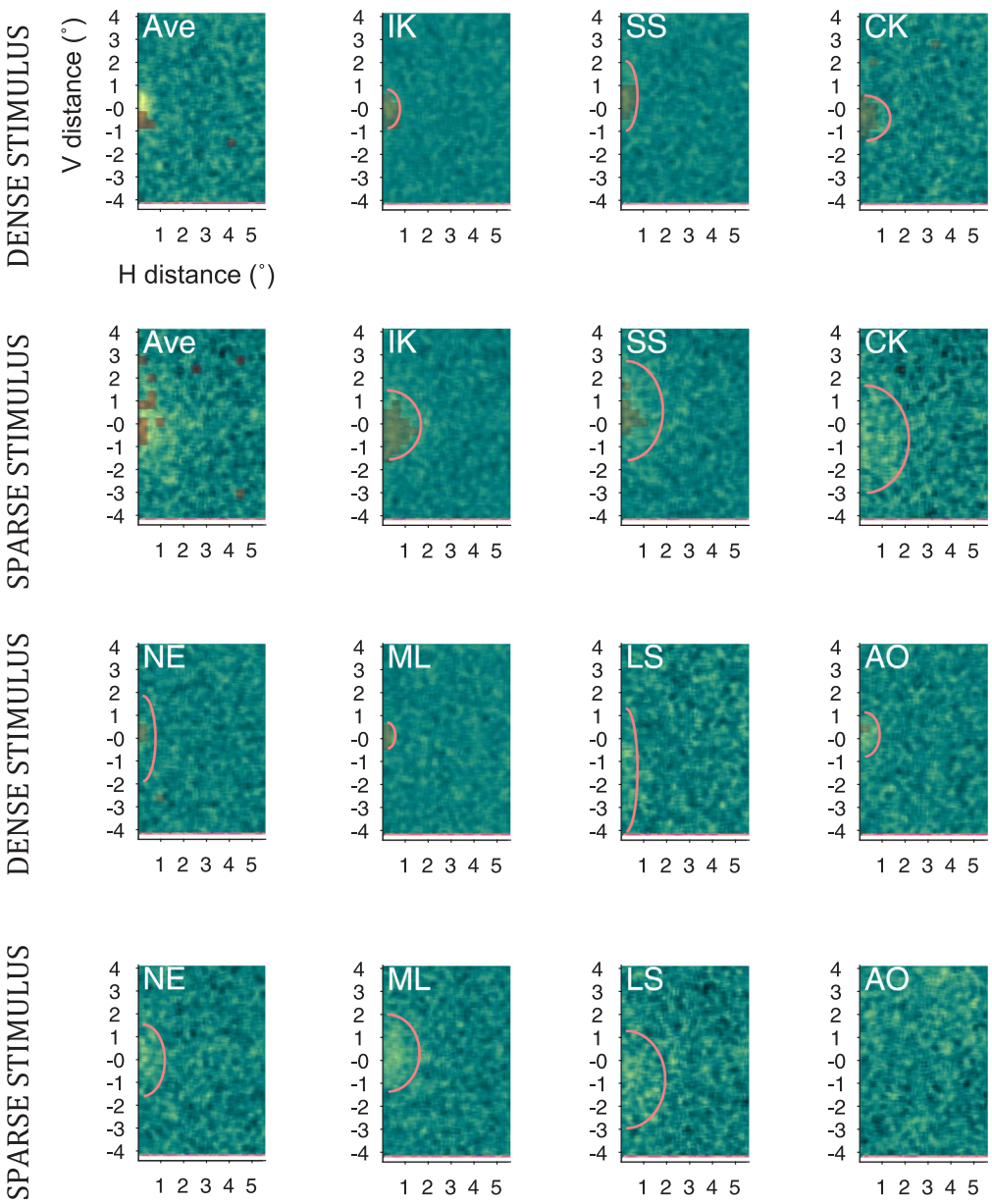

Fig. 3. Classification images. Axes show the horizontal and vertical distance from the center of the stimulus in degrees of visual angle. Yellow color indicates a high correlation (integration region), blue color low correlation. Red line represents the fitted integration region. Sparse and dense conditions are shown in separate rows. The top 2 rows show the subjects with 8800 trials and the bottom rows show the subjects with 2880 trials. Red transparent dots show the of stimulus parts with statistically significant correlations, corrected for multiple comparisons. Ave shows the average over all subjects. (For interpretation of the references to color in this figure legend, the reader is referred to the web version of this article.)

Table 1
Integration region fit parameters for individual subjects. Width, height and area are specified in degrees of visual angle. AR refers to aspect ratio.

	Dense condition				Sparse condition			
Subject	Width	Height	AR	Area	Width	Height	AR	Area
IK	0.570	0.844	1.483	1.511	1.475	1.510	1.031	7.049
SS	0.528	1.523	2.884	2.527	1.619	2.166	1.338	11.017
CK	1.124	0.987	0.878	3.487	1.938	2.351	1.213	14.316
NE	0.570	1.878	3.293	3.361	0.976	1.577	1.616	4.564
ML	0.353	0.571	1.618	0.633	1.415	1.691	1.194	7.517
LS	0.511	2.692	5.268	4.323	1.725	2.128	1.233	11.535

4. Discussion

4.1. Integration region: size and shape

The classification images revealed a single symmetry integration region that was generally highly concentrated to the center of the stimulus, elongated along the symmetry axis and roughly elliptical in shape. There was little sensitivity for symmetry near the outer border of the stimulus (except possibly for AO, sparse condition). While substantial (approximately 4 to 5-fold) variation in the estimated area of the integration region between the subjects was observed, the shape of the integration region was quite similar. These results are consistent with earlier estimates of the integration region shape (Barlow & Reeves, 1979; Dakin & Herbert, 1998; Rainville & Kingdom, 2002). However, it should be borne in mind that the integration region size (especially the elongation) may depend on observer not having any uncertainty about orientation of the symmetry axis. Note also, that these results were obtained using stimulus with discrete dots in a rectangular stimulus area. It is possible that spatial characteristics of the elements (dots or band-pass elements) and the shape of the stimulus window (rectangular, circular) may have an effect on the dimensions of the integration region. This should be explored further in future studies.

For the dense texture, the average size of the integration region was approximately 2.64 and for the sparse texture approximately 9.33 deg^2 which is consistent with the idea that the integration region covers only a small fraction of the stimulus (see for example, Jenkins, 1982).

The size of the integration region was observed to increase with

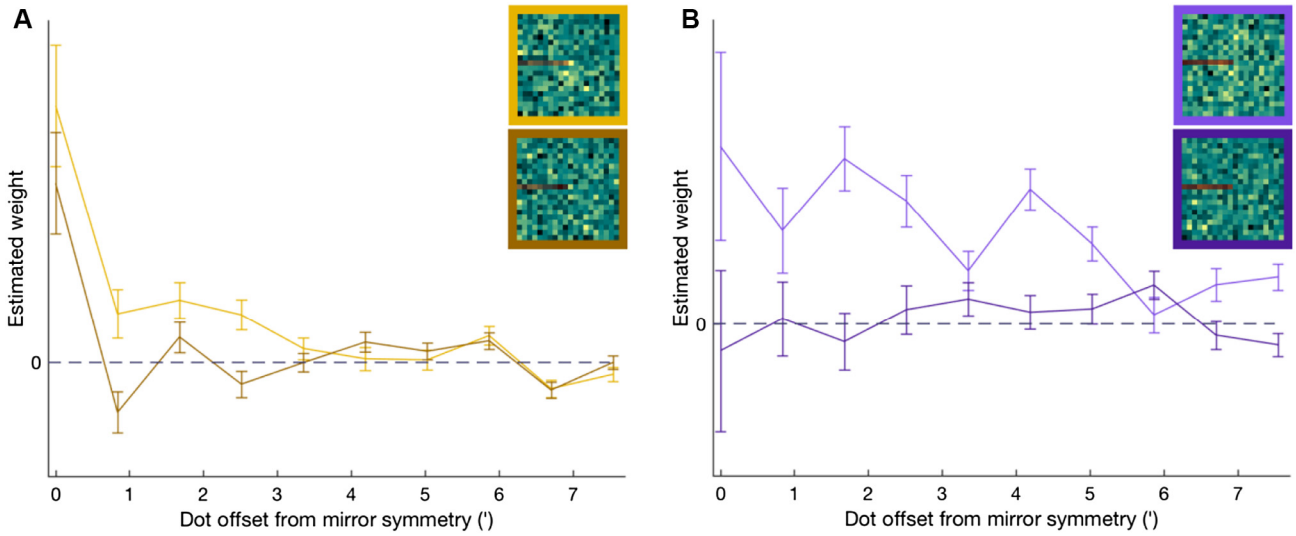

Fig. 4. Classification images for symmetry tolerance. A, Dense stimulus. B, Sparse stimulus. The tolerance classification image shows how close-to-symmetric random dots correlates with symmetry responses. The axis represents the dot pairs offset from mirror symmetry. Light color in the inset indicates that the dot offset correlates with symmetry responses. The top inset shows the classification image for symmetry tolerance inside the integration region, the bottom inset outside the integration region. Plots show the radial averages of the classification images. Light colors show the radial average that was computed from the stimulus inside the integration region, dark color outside the integration region. Error bars represents one standard error of mean.

decreasing dot density, consistent with an earlier report (Rainville & Kingdom, 2002). Why does the size of the integration area is dependent on the number of elements? One possibility is that peripheral dots are not integrated because of crowding (see e.g.: Bouma, 1970, 1973; Levi, 2008; Pelli, 2008), where neighboring, "flanking" stimulus elements distract each other in the periphery. Could crowding explain the integration region size? It is known that the distance for crowding is dependent on eccentricity, in the periphery crowding can occur over larger distances than in more foveal vision. More foveal parts of the stimulus would therefore be crowded in the dense stimulus, explaining why the integration region shrinks. It has been shown that mirror symmetry can be subject to crowding (Roddy & Gurnsey, 2011). However, it should be noted that the integration regions here were quite small (average width 1.2 and 3 deg) being mostly within the foveal vision, whereas crowding is often attributed to more peripheral vision.

Another possibility is that integration is limited by the number of symmetric "elements", similar to what has been proposed for visual short term memory (see for example: Luck & Vogel, 1997). Interestingly, Rainville and Kingdom (2002) proposed that the size of the integration region scales so that the number of elements remains constant. The results here do not directly support the idea that integration area would be directly proportional to the number of elements (dots). Multiplying the dot density by the estimated integration region yields on average 13.2 dots within the integration region in the dense condition and 3.7 in the sparse condition.

4.2. Symmetry tolerance

Symmetry tolerance classification images estimated inside the integration region showed that the matching process has rather high tolerance. The tolerance area for symmetry is centered at the perfect mirror symmetry but includes dots pairings are within about a 6 arc min tolerance. The low resolution is consistent with earlier observations that random jitter in symmetric dot positions has a minor effect on the detectability of symmetry (Barlow & Reeves, 1979). Tolerance was larger in the low-density pattern, suggesting that it may scale with dot density.

Outside the integration region, the classification image weights for symmetry tolerance were close to zero (except for the dense stimulus, 0-offset). Thus, symmetric or close-to symmetric structures outside of the integration region do not seem to contribute to the symmetry responses in any way. This suggests also, that matching outside the integration region is not merely coarser and more inefficient than inside the integration region, as had been the case if the outside classification images had shown large tolerance with little specificity for perfect symmetry. Thus, this implies that integration region is not simply a byproduct of progressively coarser matching in the periphery. Rather, it seems that symmetric structures outside the integration region do not contribute to symmetry perception at all. The reason for this foveal preference is not clear. It is possible that factors such as spatial attention to fovea may play a role here. It should be also noted that restricting symmetry integration to fovea where spatial accuracy is best may be in fact a strategy that has been developed through perceptual learning, development or evolution.

Finally, some caution should be used when generalizing the tolerance results. The task here measured the ability to detect the minimum number of symmetric dots among noise. However, in many practical scenarios it is more relevant to detect deviations from perfect symmetry. Jenkins (1983) showed that the visual system can efficiently detect small deviations from symmetry. It is quite possible that the tolerance region for this kind of tasks where the critical information would not be in the maximal detection of perfectly symmetric dots, but detection of deviations, would result in a different tolerance classification image (presumably tuned to offsets from symmetry).

4.3. Efficiency and versatility of symmetry perception

The results here indicate that the efficiency of symmetry perception is restricted by a spatially limited integration area and the low resolution of the matching process. A statistically optimal symmetry detector would compare all stimulus elements when evaluating the symmetry. How can a large part of the human inefficiency can be explained by a limited integration region? This was investigated by simulations, using an ideal observer. First, an ideal observer based the response on the number of perfectly symmetric dots, integrated over the whole stimulus area. For both stimuli, the observer absolute efficiency (the square of the ratio of observer d′ to ideal observer d′) was found to be very low. For the dense stimulus the average was 0.00044 (maximum 0.00057; minimum 0.00037). For the sparse stimulus the average was 0.00042

(maximum 0.00057; minimum: 0.00028). The difference was not statistically significant ($t(6) = -0.498; p > 0.05$). Next, an ideal observer that used an oval-shaped integration region whose size was matched with human data, was used. Mean efficiency was on average 0.014 for the dense and 0.0034 for the sparse stimulus (or approximately 34 and 8 times higher, respectively) which is still approximately 100 times better than human efficiency. Thus, the limited integration region alone cannot explain the human inefficiency, and other inefficiencies such as non-ideal symmetry matching (as shown in the symmetry tolerance classification image) and internal noise play a major role.

It should be noted that the efficiency compared to the whole stimulus ideal observer was approximately the same in both sparse and dense conditions. The performance of an ideal observer increases with stimulus size; it would predict that performance in sparse condition with larger integration region would be higher. However, human detection performance was the same in both conditions. This implies that the human efficiency relative to integration area is lower in sparse condition. The reason for this is not clear, but it is possible that there is more uncertainty about the location of the symmetry axis in the sparse condition that could reduce the resolution and efficiency of symmetry matching. This is also suggested by the fact that the sparse symmetry tolerance classification image had larger tolerance.

5. Conclusions

This study showed that a classification image method can be used to investigate processing of bilateral symmetry in the visual system. The method permits a direct means to estimate the symmetry integration region, which was found to be elongated along the symmetry axis and concentrated to the center of the stimulus and very compact (3–9 deg^2). Thus, the results give support for the idea that symmetry is estimated from a very small region of stimulus, or a very small number of dots. However, the size of the integration region was dependent on the stimulus density, being larger with the sparse stimulus. This suggests that the symmetry integration region is not solely determined by low-level neural factors, such as size of the fovea or spatial frequency sensitivity. On the other hand, the size of the integration region was not directly proportional to the number of dots, as would be expected in an element-based integration limit.

A further tolerance analysis probed the resolution of symmetry matching in various parts of the stimulus, providing a new way to estimate the tolerance in symmetry matching across the different parts of the stimulus. The matching process was found to have rather low resolution (about 6 arc min tolerance). Outside the integration region we did not find evidence for even poor symmetry matching, which suggests that peripheral symmetry signals are not lost because of low matching efficiency.

One possibility is that integration region size is limited by crowding in the periphery, but more studies will be needed to test this idea.

Acknowledgements

The author would like to thank Dr. Jussi Saarinen, Tarja Peromaa and two anonymous reviewers for comments and Mr. Erik Leichter for assisting in experiments.

References

Ahumada, A. J. (2002). Classification image weights and internal noise level estimation. *Journal of Vision, 2*(1), 121–131 10:1167/2.1.8.

Alp, N., Kohler, P. J., Kogo, N., Wagemans, J., & Norcia, A. M. (2018). Measuring integration processes in visual symmetry with frequency-tagged EEG. *Scientific Reports, 8*(1), 1–11. https://doi.org/10.1038/s41598-018-24513-w.

Bahnsen, P. (1928). Eine Untersuchung über Symmetrie und Asymmetrie bei visuellen Wahrnehmungen. *Zeitschrift Für Psychologie, 108*, 129–154.

Barlow, H., & Reeves, B. (1979). The versatility and absolute efficiency of detecting mirror symmetry in random dot displays. *Vision Research, 19*, 783–793.

Beard, B. L., & Ahumada, A. J. (1996). Perceptual classification images from Vernier acuity masked by noise. *Perception, 26*, S18.

Benjamini, Y., & Hochberg, Y. (1995). Controlling the false discovery rate: A practical and powerful approach to multiple testing. *Journal of the Royal Statistical Society B, 57*(1), 289–300. https://doi.org/10.2307/2346101.

Bertamini, M., Silvanto, J., Norcia, A. M., Makin, A. D. J., & Wagemans, J. (2018). The neural basis of visual symmetry and its role in mid- and high-level visual processing. *Annals of the New York Academy of Sciences,* 1–16. https://doi.org/10.1111/nyas.13667.

Bona, S., Herbert, A., Toneatto, C., Silvanto, J., & Cattaneo, Z. (2014). The causal role of the lateral occipital complex in visual mirror symmetry detection and grouping: An fMRI-guided TMS study. *Cortex, 51*(1), 46–55. https://doi.org/10.1016/j.cortex.2013.11.004.

Bouma, H. (1970). Interaction effects in parafoveal letter recognition. *Nature, 226*, 177. https://doi.org/10.1038/226177a0.

Bouma, H. (1973). Visual interference in the parafoveal recognition of initial and final letters of words. *Vision Research, 13*(4), 767–782. https://doi.org/10.1016/0042-6989(73)90041-2.

Brainard, D. H. (1997). The psychophysics toolbox. *Spatial Vision, 10*(4), 433–436.

Dakin, S. C., & Herbert, A. M. (1998). The spatial region of integration for visual symmetry detection. *Proceedings of the Royal Society of London - Series B: Biological Sciences, 265*(1397), 659–664. https://doi.org/10.1098/rspb.1998.0344.

Eckstein, M., & Ahumada, A. (2002). Classification images: A tool to analyze visual strategies. *Journal of Vision, 2*(1), i.

Efron, B., & Tibshirani, R. J. (1993). *An introduction to the bootstrap.* New York: Chapman & Hall.

Jenkins, B. (1982). Redundancy in the perception of bilateral symmetry in dot textures. *Perception & Psychophysics, 32*(2), 171–177. https://doi.org/10.3758/BF03204276.

Jenkins, B. (1983). Component processes in the perception of bilaterally symmetric dot textures. *Perception & Psychophysics, 34*(5), 433–440. https://doi.org/10.3758/BF03203058.

Jenkins, B. (1985). Orientational anisotropy in the human visual system. *Perception & Psychophysics, 37*(2), 125–134. https://doi.org/10.3758/BF03202846.

Julesz, B. (1971). *Foundations of cyclopean perception.* Chicago: University of Chicago Press.

Kleiner, M., Brainard, D. H., & Pelli, D. G. (2007). What's new in Psychtoolbox-3? *Perception, 36*(ECVP Abstract Supplement).

Knoblauch, K., & Maloney, L. T. (2008). Estimating classification images with generalized linear and additive models. *Journal of Vision, 8*(16), 1–19. https://doi.org/10.1167/8.16.10.Introduction.

Knoblauch, K., & Maloney, L. T. (2012). *Modeling psychophysical data in R.* New York, NY: Springer New York 10.1007/978-1-4614-4475-6.

Levi, D. M. (2008). Crowding-An essential bottleneck for object recognition: A mini-review. *Vision Research, 48*(5), 635–654. https://doi.org/10.1016/j.visres.2007.12.009.

Luck, S. J., & Vogel, E. K. (1997). The capacity of visual working memory for features and conjunctions. *Nature, 390*(6657), 279–281. https://doi.org/10.1038/36846.

Machilsen, B., Pauwels, M., & Wagemans, J. (2009). The role of vertical mirror symmetry in visual shape detection. *Journal of Vision, 9*(12), 1–11. https://doi.org/10.1167/9.12.11.Introduction.

Murray, R. F. (2011). Classification images: A review. *Journal of Vision, 11*(5), 1–25.

Neri, P., Parker, A. J., & Blakemore, C. (1999). Probing the human stereoscopic system with reverse correlation. *Nature, 401*, 695–698.

Pelli, D. G. (1997). The VideoToolbox software for visual psychophysics: Transforming numbers into movies. *Spatial Vision, 10*(4), 437–442.

Pelli, D. G. (2008). Crowding: A cortical constraint on object recognition. *Current Opinion in Neurobiology, 18*(4), 445–451. https://doi.org/10.1016/j.conb.2008.09.008.

Rainville, S. J. M., & Kingdom, F. A. A. (2002). Scale invariance is driven by stimulus density. *Vision Research, 42*(3), 351–367. https://doi.org/10.1016/S0042-6989(01)00290-5.

Rhodes, G. (2006). The evolutionary psychology of facial beauty. *Annual Review of Psychology, 57*(1), 199–226. https://doi.org/10.1146/annurev.psych.57.102904.190208.

Roddy, G., & Gurnsey, R. (2011). Mirror symmetry is subject to crowding. *Symmetry, 3*(3), 457–471. https://doi.org/10.3390/sym3030457.

Sasaki, Y., Vanduffel, W., Knutsen, T., Tyler, C., & Tootell, R. (2005). Symmetry activates extrastriate visual cortex in human and nonhuman primates. *Proceedings of the National Academy of Sciences of the United States of America, 102*(8), 3159–3163. https://doi.org/10.1073/pnas.0500319102.

Treder, M. S. (2010). Behind the looking-glass: A review on human symmetry perception. *Symmetry, 2*(3), 1510–1543. https://doi.org/10.3390/sym2031510.

Tyler, C. W., Baseler, H. A., Kontsevich, L. L., Likova, L. T., Wade, A. R., & Wandell, B. A. (2005). Predominantly extra-retinotopic cortical response to pattern symmetry. *NeuroImage, 24*(2), 306–314. https://doi.org/10.1016/j.neuroimage.2004.09.018.

van der Helm, P. A. (2015). Symmetry perception. In J. Wagemans (Ed.). *The Oxford handbook of perceptual organization* (pp. 108–128). Oxford, United Kingdom: Oxford University Press.

Wagemans, J. (1997). Characteristics and models of human symmetry detection. *Trends in Cognitive Sciences, 1*(9), 346–352. https://doi.org/10.1016/S1364-6613(97)01105-4.

Watson, A. B., & Pelli, D. G. (1983). QUEST: A Bayesian adaptive psychometric method. *Perception and Psychophysics, 33*, 113–120.

Wenderoth, P. (1997). The role of implicit axes of bilateral symmetry in orientation processing. *Australian Journal of Psychology, 49*(3), 176–181. https://doi.org/10.1080/00049539708260463.